Isomorphic silicon/aluminum substitution on layered ilerite – Structural study and calorimetry of copper interaction

ARTICLE *in* MICROPOROUS AND MESOPOROUS MATERIALS · NOVEMBER 2012

Impact Factor: 3.45 · DOI: 10.1016/j.micromeso.2012.06.040

3 AUTHORS:

Cléo Pires
Instituto Tecnologico de Aeronautica
11 PUBLICATIONS **45** CITATIONS
SEE PROFILE

José R. Costa
University of Campinas
1 PUBLICATION **2** CITATIONS
SEE PROFILE

Claudio Airoldi
University of Campinas
482 PUBLICATIONS **8,440** CITATIONS
SEE PROFILE

Microporous and Mesoporous Materials 163 (2012) 1–10

Contents lists available at SciVerse ScienceDirect

Microporous and Mesoporous Materials

journal homepage: www.elsevier.com/locate/micromeso

Isomorphic silicon/aluminum substitution on layered ilerite – Structural study and calorimetry of copper interaction

Cléo T.G.V.M.T. Pires, José R. Costa, Claudio Airoldi *

Institute of Chemistry, University of Campinas, Unicamp, P.O. Box 6154, 13084-971 Campinas, SP, Brazil

ARTICLE INFO

Article history:
Received 19 December 2011
Received in revised form 5 June 2012
Accepted 23 June 2012
Available online 30 June 2012

Keywords:
Layered silicate
Isomorphic substitution
Copper sorption
Calorimetry
XAFS

ABSTRACT

Layered ilerite (Na-il) and ilerite with structural aluminum incorporated (Na–[Al]il) through isomorphic substitution of silicon atom in the silicic network were synthesized by hydrothermal procedures. X-ray diffraction (XRD) and scanning electron microscopy confirmed the structure and morphology. The incorporated metal was detected and quantified by nuclear magnetic resonance in the solid state and X-ray fluorescence. Both classes of materials sorbed copper and these interactions were calorimetrically followed through isothermal titrations. The thermodynamic data for Na-il and Na–[Al]il gave ΔG -4.2 ± 0.4 and -4.7 ± 0.5 kJ mol^{-1}, ΔH 1.54 ± 0.02 and 2.9 ± 0.01 kJ mol^{-1} and ΔS 19 ± 1 and 25 ± 1 J K^{-1} mol^{-1}, respectively. These values are relatively close and the differences are explained by the higher acidity for the Na–[Al]il surface, which leads to stronger interaction between the copper species and the solid material. The copper-ilerite structures were characterized by XRD, the environment surrounding copper has been studied by X-ray absorption spectroscopy and EXAFS was used to determine copper coordination, metal–metal and copper-oxygen distances. For both materials octahedral coordination was determined, whose axial and equatorial distances for Cu–O gave 196 and 234 pm for Na-il, respectively. For the Na–[Al]il sample two equatorial distances, 189 and 196 ppm and an axial distance of 247 pm were found. These results indicate that hydrated Cu^{2+} species interact with silicate layers by electrostatic forces. The XAS results are in agreement with the calorimetric results and with acid–base principles, as well described for these systems.

1. Introduction

Ilerite, also known as octosilicate or RUB-18, is a well-organized layered hydrated silicate that naturally occurs or can be synthesized through hydrothermal procedures [1]. This structurally self-arranged compound is one of the hydrous layered silicate members containing sodium that also include makatite, kanemite, magadiite and kenyaite [2]. The interlayer cavity space includes hydrated cations, usually sodium or hydrogen, to maintain charge neutrality. These internal ions can be exchanged by charged inorganic or organic species. In a similar way as happens with zeotype materials, the lamellar structure can be slightly modified by the isomorphic substitution of silicon by other atoms, such as iron, aluminum or titanium [3]. The isomorphic chemical exchange in the original structure causes some surface property modifications in agreement with the new atom incorporated and also its degree of concentration.

The synthesized ilerite in sodium form, (Na-ilerite), has precise and normal structure and a determined chemical composition [4]. Thus, its unit cell has the formula $Na_8Si_{32}O_{64}(OH)_8{\cdot}32H_2O$, with an interlayer distance and a layer thickness of 1.10 and 0.73 nm, respectively, indexed as (001) diffraction planes, with the crystal structure details elucidated also by X-ray diffraction patterns and solid-state NMR spectroscopy [1,5]. The secondary structural building units of Na-ilerite silicate layer consists of four- and five-membered rings. This kind of [54] cage, common for many zeolites, was observed for the first time in a layered silicate. The remaining silicon atoms are bonded to hydroxyl groups or have a negative charge that is compensated by octahedral coordinated sodium cations. Weak and strong hydrogen bonds among the structural water and siloxane or silanol groups are expected [6].

Structural aluminum inserted throughout the silicate network increases the layer acidity due to the misbalance in charge. Aluminosilicate materials have a wide range of potential applications, mainly as catalysts and sorbents in many reactions and separation uses [7]. For example, layered silicate materials with aluminum have already been synthesized for magadiite and ilerite structures [3,8]. For magadiite the metal inserted into the silicic network was successfully investigated by ^{27}Al NMR spectra. On the other hand, gallium containing samples were also synthesized, with the majority of this element remaining as oxide in the interlayer space [3]. It is worth to mention that ilerite samples containing structural aluminum or tin inserted were not obtained, but magadiite was

* Corresponding author.
E-mail address: airoldi@iqm.unicamp.br (C. Airoldi).

1387-1811/$ - see front matter © 2012 Elsevier Inc. All rights reserved.
http://dx.doi.org/10.1016/j.micromeso.2012.06.040

obtained instead, with small amounts of the metal in the tetrahedral sites and oxides on the surface or in the interlayer spaces [8].

Among the metal contaminants, copper is one of the most investigated in sorption processes, due to its toxicity in Wilson disease and damage to the gastro-intestinal tract, followed by its abundance as contaminant in many environments and also its many chemical applications [9]. In this context, zeolites and other silica materials containing exchanged copper cations have activity in nitrous oxide catalytic decompositions [10], catalytic conversion of methane to methanol [11] and wet hydrogen peroxide catalytic oxidation, among other applications [12].

Investigations involving interactive copper processes with many sorbents can be performed by some techniques, but the thermodynamic data can be obtained from isothermal calorimetric titration by a direct measurement [13,14]. These data are closely correlated with solid–liquid interface interactions and the effect of isomorphic substitutions and other modifications can be clearly shown. In addition, the use of X-ray absorption spectroscopy for samples after sorption processes also aids the elucidation of this kind of process and mainly the metal species characterization on the final material [15,16].

Taking into account investigations associated with ilerite, not only involving clay science, but also due to structural similarities with the zeolite field, are relevant and can give outstanding contributions to better understanding of some processes. Thus, the purpose of the present study is to synthesize and characterize layered ilerite samples containing aluminum, followed by the investigation of copper sorption processes at the solid/liquid equilibrium, to elucidate the exchange effect of this cation in this well-organized solid derivative of silicic acid.

2. Experimental

2.1. Chemicals

Silica gel, aluminum isopropoxide and copper nitrate were purchased from Aldrich and sodium hydroxide from Synth. All reagents were used as supplied.

2.2. Synthesis

Sodium ilerite silicate was synthesized as previously described [17]. Aluminum containing samples were made by a similar method, but aluminum alkoxide was added before hydrothermal treatment. The gel composition in molar ratio was established as $0.025Al_2O_3$:SiO_2:0.5NaOH:7.0H_2O and reactions were done inside a Teflon-lined autoclave at 378 K from 3 to 9 days. The obtained solids were washed with distilled water until neutrality and dried at room temperature. The series of named synthesized layered sodium ilerites (Na-il) and, when containing aluminum (Na–[Al]il), is followed by a number that corresponds to the hours in the experimental preparation procedure, for example, Na–[Al]il-216 indicates that the compound was synthesized using 216 h in the autoclave.

2.3. Characterization

X-ray powder diffraction patterns (XRD) for solids were performed with a Shimadzu XRD-7000, using CuKα radiation (40 kV, 30 mA), at a scan rate of 2° 2θ min^{-1}.

Solid state nuclear magnetic resonance (NMR) spectra were performed in a Bruker 400 Avance II + spectrometer in a zirconium rotor at 10 kHz of resolution with magic-angle spinning (MAS). The ^{27}Al 3Q-MAS NMR was recorded at 104.3 MHz. The pulse length was 1.0 μs, repetition time of 2.0 s, with reference to $Al(NO_3)_3$ as 0 ppm. These values were calibrated for a $\pi/20$ magnetization flip angle. Triple-quantum experiments were performed by means of two strong pulses and a MAS frequency of 12.5 kHz. Correlation maps of ^{27}Al 1Q and ^{27}Al 3Q spectra were constructed to determine precisely the number of sites. For ^{1}H and ^{29}Si nuclei the FSLG-CP–HETCOR experiment was performed with contact time of 5.0 ms and repetition time of 2 s. For copper containing samples cross-polarization (CP) MAS ^{29}Si spectra were obtained at 59.61 MHz with pulse repetition and contact time of 3 s and 3 ms, respectively.

The thermogravimetric (TG) data were obtained in a TA Instruments 5100 with heating up to 1273 K at 0.167 K s^{-1} heating rate under an synthetic air flow of 1.67 cm^3 s^{-1}.

Scanning electron microscopy (SEM) images were obtained after dispersing the samples in acetone with an ultrasound bath, drying on a stub and then coating with gold. The images were performed in a Jeol 6360-LV, operating at 15 kV.

Energy dispersion spectroscopy (EDS) for chemical compositions were also analyzed with a Noran System Six coupled to a microscope. Elemental mapping images and numerical data for quantifications were carried out in triplicate with the ZAF method.

Nitrogen sorption at low temperature was performed in a volumetric ASAP 2010 Micromeritrics analyzer at 77 K. Surfaces areas were calculated by the Brunauer-Emmett-Teller (BET) method.

For transmission electron microscopy (TEM) the samples were dispersed in isopropanol with an ultrasound bath, then a drop of this dispersion was dropped onto a copper grid with a carbon film and the measurements were performed in a JEM 3010, operating at 300 kV.

X-ray fluorescence (XRF) measurements were performed using bench-top Shimadzu EDX 700 equipment provided by a rhodium tube operated at a maximum voltage of 50 kV. The measurements were performed in 30 Pa vacuum, 25% detector dead time, 10 mm beam collimation and 100 s irradiation times. Calibration samples with weighed silicon, sodium and aluminum oxides were prepared and analyzed.

2.4. Sorption

Copper sorption were carried out by the batchwise method with $Cu(NO_3)_2$ at 298 ± 1 K. For this purpose samples of approximately 20 mg were suspended in a series of flasks containing aqueous copper solutions, varying in concentration from 0.12 to 8.0 mmol tdm^{-3}, with deionized water with pH near to 5. Samples were left under stirring for 24 h and the amount of copper ions in the supernatant was measured using a Perkin Elmer model 3000 DV (ICP-OES), at 1.3 kW with 1.67×10^{-2} cm^3 s^{-1} of solution flow rate and argon flow rate of 0.30 dm^3 s^{-1}. The obtained data was adjusted to the Langmuir, the Freundlich and the Tenkim models [18], to estimate the monolayer sorption capacity of each sample.

2.5. Calorimetry

Isothermal calorimetric titrations with copper were followed on a differential isothermal LKB 2277 microcalorimetric system, using almost 20 mg of each sample suspended in 2.0 cm^3 of deionized water inside a stainless steel vessel, which was stirred at 298.15 ± 0.20 K [13]. After reaching equilibrium, aliquots of copper cation solution were added through a microsyringe coupled to the calorimetric vessel. The thermal effect of each added increment was recorded and the end of the titration was indicated by a constant thermal effect. The same procedure was used to determine the dilution effect, combining these heat outputs to determine the net value. The results were used to obtain the enthalpy and adjusting the data with sorption models all thermodynamic parameters can be determined [13].

2.6. X-ray absorption

X-ray absorption (XAS) measurements were obtained with the XAFS beam line on Max Lab (1.5 GeV). The experiments were made with CuK-edge and a Si (1 1 1) monochromater was used. Its calibration was performed by assigning the energy value of 8979 eV to the first inflection point observed for the absorption edge of a copper foil, which was recorded simultaneously between the second and a third ionization chamber, to calibrate the energy of the monochromator. Spectra for Cu-il and Cu–[Al]il samples were acquired in the transmission mode at room temperature. The scans were individually calibrated and then averaged for fitting. At least three scans were recorded for the sample and model compounds in the 8900–10,000 eV energy range.

The EXAFSPAK computational program package [19] was employed for XAS spectra treatment and data fitting. The background sorptions were subtracted by fitting a straight line through the pre-edge region from each averaged raw spectrum. In the EXAFS region, the background subtractions were done by automatically fitting strong high spline clamps through the region and the data above the edge had these fits subtracted. The threshold energies were selected arbitrarily at maxima μ(E) (8991 eV). The c(k) was extracted using cubic splines and a k^2 weighted EXAFS spectrum was Fourier transformed to *R*-space in the 200–1250 pm^{-1} range with a Hanning window. In the case of Cu-il and Cu–[Al]il sample spectra, the contribution of coordination shells (Cu-O and Cu–Cu) were extracted by back Fourier transforms in *R* space and then fitted using theoretical standard phases and amplitude functions determined with the FEFF 7.0 computational program [20]. The fittings were performed in the *R*-space by Fourier transforming both the experimental data and the FEFF theoretical function [20].

3. Results and discussion

3.1. Ilerite synthesis

X-ray diffraction patterns of ilerite samples are shown in Fig. 1. Pure silica samples start their crystallization after 3 days of hydrothermal treatment, as given by very low signals (curve a). After 6 days the ilerite structure is already obtained (curve b), presenting all characteristic diffraction signals [4], however, part of it remains in amorphous phase. Finally, the pure octosilicate structure is obtained after 9 days of reaction (curve c).

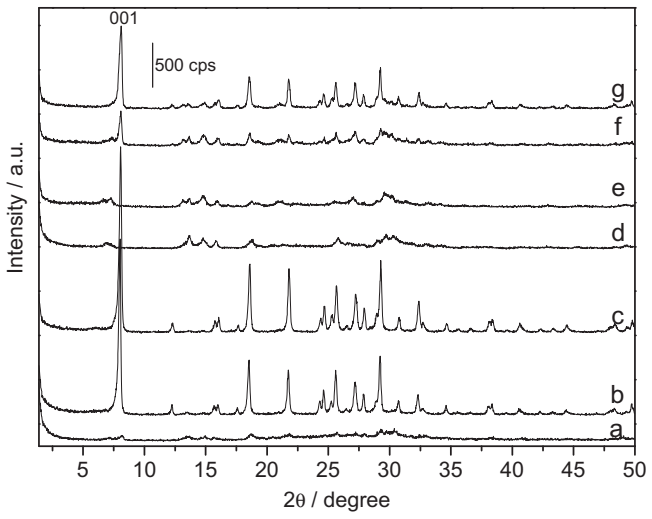

Fig. 1. Na-ilerite XRD patterns: Na-il-72 (a), Na-il-144 (b), Na-il-216 (c), Na–[Al]il-72 (d), Na–[Al]il-120 (e), Na–[Al]il-144 (f) and Na–[Al]il-216 (g).

Aluminum insertion into the original structure gives a crystallization pathway in another direction. A pre-phase formation was observed with peaks that correspond to other layered materials formed with larger basal distances (curves d and e) and other peaks that suggested the presence of unfavorable organized magadiite structure [3,8]. Both structures have similarities, but magadiite lamella thickness is wider than ilerite. After 6 days the ilerite peaks started to be noticed (curve f), indicating an ilerite co-crystallization process and all previous silicic acid magadiite was converted into ilerite after 9 days (curve g), as observed verified by the absence of the characteristic diffraction signals of the magadiite layered compound. The peaks at 2θ 13.2°, 13.6° and 14.7° are due to scattering related to the interatomic vectors amorphous materials for curve g [4,21–23]. These reflections are also present with very low intensity for Na-il-216 (curve c), which indicate that ilerite aluminosilicate presents amorphous regions at higher concentration than pure layered silicate.

These differences relate to the amorphous silicate amount for each material and reflect also the surface area for each sample. For example, Na-il-216 and Na-[Al]-216 samples gave surface areas of 18 and 43 $m^2\,g^{-1}$, respectively, the difference being due to the presence of a small amount of amorphous silica, which usually has surface areas around 600 $m^2\,g^{-1}$.

Diffraction signals at smaller angles around 2θ 8.0° represent the Na-il d_{001} plane with 1.1 nm of basal distance, for pure silicate and aluminum-containing samples, where few changes were observed. This peak position increases up to 2θ 8.1°, indicating a slight basal distance decrease due to aluminum incorporation. This behavior increased the interaction strength between the lamella and hydrated sodium cations and decreased the interlayer spacing. The peaks at higher angles are related to lamellar structure features and also confirm that the ilerite structure was synthesized [4].

Scanning electron microscopy images shown ilerite sample morphologies in Fig. 2 and both samples presented a typical layered plate-like form, in agreement with previous results [24]. The difference in morphology between pure silicate ilerite for Na-il-216 from now Na-il and aluminosilicate ilerite Na–[Al]il-216, hence for Na–[Al]il) is related to higher plate agglomeration degree for the first silicate. The average crystal size, about 2.2 × 3.4 μm and 3.2 × 5.8 μm at $a \times b$ directions were obtained for this sequence of ilerites. However, some larger crystals were observed with up to 12 μm at the greatest dimension. These results also indicate two different crystallization pathways, as suggested by XRD results.

The observed plate thickness for both samples were variable from a few tens of nanometers up to almost one micron, but in comparing samples, pure silicate ilerite is thinner, probably due to the stronger interaction between the layers and the presence of hydrated sodium for Na–[Al]il.

Aluminum incorporation was quantified by X-ray fluorescence (XRF) data and energy dispersive spectroscopy (EDS) and presented very close results while thermogravimetric (TG) data demonstrated the hydration degree. Thus, Na–[Al]il presented 1.2% and 1.4% of aluminum by XRF and EDS, respectively, and combed with TG results, the ilerite formula was deduced as $Na_{9.4}Al_{1.4}Si_{30.6}O_{64}(OH)_{9.4}{\cdot}36H_2O$.

The crucial measurement to confirm the aluminum insertion in the silica network is given by NMR spectroscopy. The correlation maps of ^{29}Si–1H and ^{27}Al with triple quantum spectra of Na–[Al]il, are shown in Fig. 3. For silicon spectra, three different chemical shifts were noticed at −94.5, −99.6 and −110.9 ppm, related to Q^2, Q^3 and Q^4, respectively. Pure silicon ilerite contains Q^3 and Q^4 species [5,25], but the isomorphic substitution of aluminum in the silicate network again gave both these signals and generated the Q^2 signal. It is observed also that the hetero-

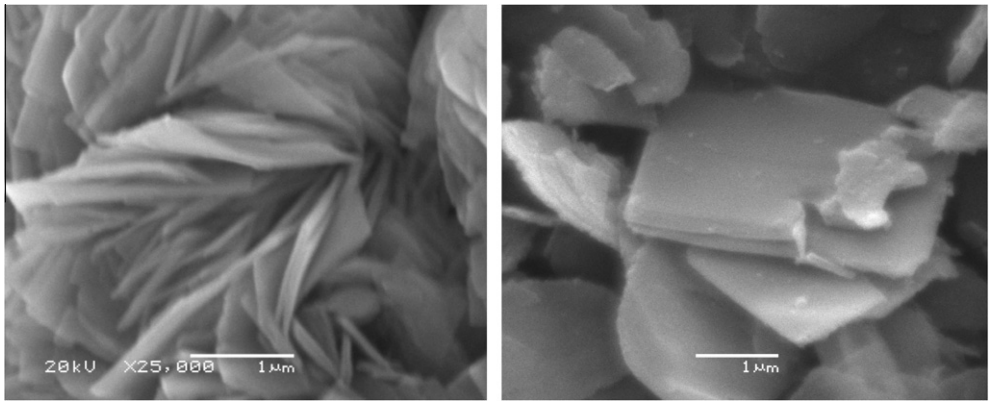

Fig. 2. SEM micrographies of Na-il-216 (a)and Na–[Al]il-216 (b) samples.

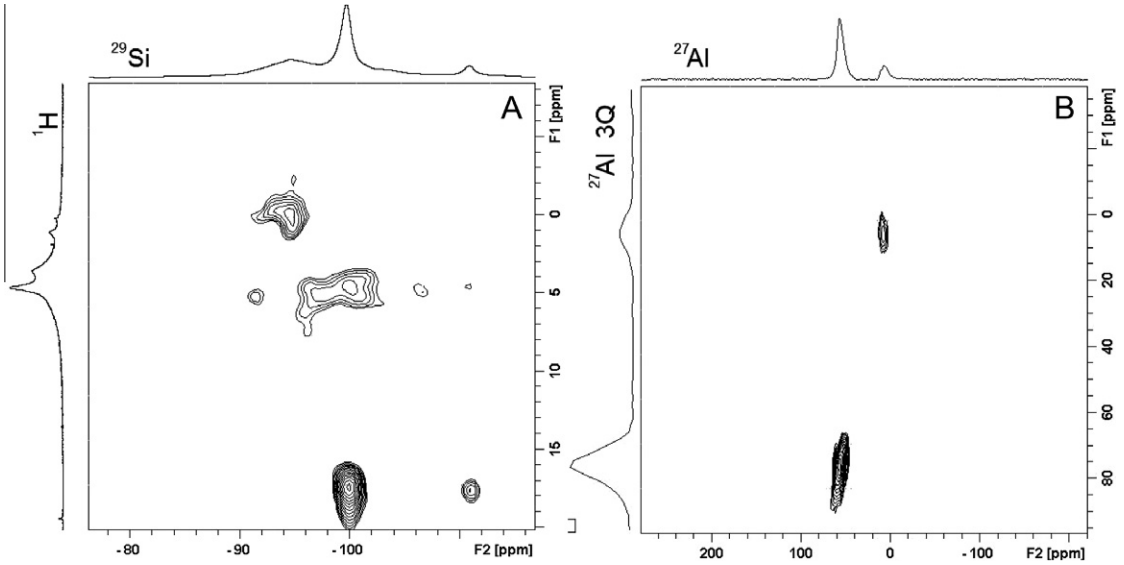

Fig. 3. NMR results for Na–[Al]il-216 sample. A) ^{29}Si vs ^{1}H FSLG-CP-HETCOR experiment and B) ^{27}Al 3Q-MAS correlation map.

atom significantly increases the Q^3 sites. Thus this result is a strong indication of aluminum isomorphic substitution inside the ilerite layer structure.

Proton NMR spectra showed three main chemical shifts centered at 1.1, 3.6 and 4.7 ppm, which represent hydrogen of water molecules in different positions on the surface of the bulk and in the interlayer space, and also due to the hydrogen from silanol groups, respectively [25,26]. The correlation between hydrogen bond lengths as determined from diffraction studies and ^{1}H chemical shift [27] predicts an H···O bridging bond length in the 0.15–0.16 nm range for the octosilicate.

To support the assignment of the proton NMR signals and to verify different silicon sites, two dimension (D) cross polarization (CP) experiment correlating ^{1}H and ^{29}Si chemical shifts were performed. On applying the $^{1}H/^{29}Si$ CP sequence, the resulting 2D data matrix directly correlates those ^{1}H and ^{29}Si nuclei, in which CP takes place, as shown in Fig. 3A. The result illustrates that all protons giving rise to the signals centered at 3.6 and 4.7 ppm were efficiently cross polarized to silicon Q^3 and Q^4 signals, while the signal at 1.1 ppm is strongly related with the Q^2 site. A total of five different silicon sites were obtained, being two Q^2, two Q^3 and one Q^4. These results are in complete agreement with the aluminum isomorphic substitution situation into the ilerite structure, which have just one Q^3 and one Q^4 for pure silica composition [28]. Substitutions in the Q^4 sites generate a Q^2 and new kind of Q^3, while the aluminum insertion at Q^3 sites generates a different Q^2.

Aluminum multiple quantum experiments were performed in order to distinguish distinct sites regarding the geometry. ^{27}Al spectra, shown in Fig. 3B, present signals for tetrahedral species at 56.8 and 76.7 ppm and for octahedral species at 6.9 and 5.8 ppm for single and triple quantum spectra, respectively. The chemical shift ratio Al_{Td} /Al_{Oh} found was 4.3, which represent 82% tetrahedrically coordinated aluminum that have perfect positions for ilerite layer structure, as suggest by ^{29}Si NMR results. The hexacoordinated aluminum signal is attributed to the presence of framework aluminum coordinated by two water molecules in the crystal corners or on defects [29]. The correlation multiple quantum map reveals that each geometric aluminum coordinated is related just with its own geometry, thus basically two aluminum sites are presented. The combination results of XRD, ^{29}Si and ^{27}Al NMR with the obtained composition by XRF and TG conclude that the achievement of Na–[Al]il with good crystallinity and structural aluminum was obtained.

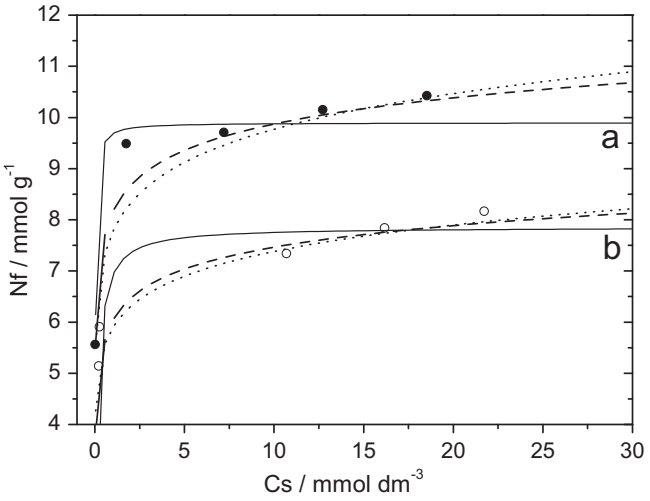

Fig. 4. Copper sorption equilibrium for Na-il-216 (a)and Na–[Al]il-216 (b). These data were adjusted to the Langmuir (—), the Freundlich (·····) and the Temkin (- - -) isotherm models at 298 ± 1 K.

3.2. Copper sorption and calorimetry

The presence of silanol groups on the ilerite surface function as acid sites to perform sorption. Through the bathwise process the amount of copper cation uptake from solution at the solid/liquid interfaces was evaluated, which amount is adjusted to the following expression:

$$N_f = (n_i - n_s)/m \quad (1)$$

where N_f is the number of moles sorbed on ilerite, n_i and n_s the number of moles of copper at the beginning of the experiment and after reaching equilibrium, and m is the mass of sorbent material for each point [30,31]. The sorption isotherms were obtained by plotting N_f against the concentration of cation in the supernatant at equilibrium (Cs), which data was obtained from ICP-OES analyses, as shown Fig. 4. The isotherms were fitted to the Langmuir, the Freundlich and the Temkin models. It is well established that layered silicates and aluminosilicates, such as zeolites, have exchangeable counter balance extra framework cations, that sodium is present in this case [5,17].

For this sorption process, copper cations substitute the sodium position and also can interact with other silanol groups available in crystal defects and in free structural corners of the compound. The data from sorption isotherms gave maximum values of 10.1 ± 0.2 and 8.4 ± 0.1 mmol g^{-1} for Na-il and Na–[Al]il, respectively, as shown in Table 1. The higher maximum sorption value for pure silica ilerite is explained by the crystal morphology, which is thinner than aluminum containing samples and, consequently, make it easier for sodium to be exchanged by copper cations, as also verified by the obtained equilibrium constants, as listed in Table 1, with higher values for Na-il.

Despite Na–[Al]il presenting higher surface area than Na-il, its metal sorption capacity is lower, which indicates a diffusion driven process or a stronger interaction among lamella silanol groups with the copper cations than that present on an amorphous silica surface.

For both samples all three equilibrium models fitted very well for copper sorption isotherms, presenting high determination coefficients, reaching 0.98 and 0.96 for the Temkin model for Na-il and Na–[Al]il, respectively, with higher R^2 values for other models, indicating a better sorption process for adjusting data. The relative discrepancies on constant ratios between Na-il and Na–[Al]il obtained by the different models, the better adjustment of the Temkin and the magnitude of the values indicate an ionic exchange process, with some precipitation or other simultaneous event. For all cases, the constants obtained were higher than unity which means a favorable process, considering a homogeneous, heterogeneous or interactive surface for the sorbing species [18].

Calorimetric isotherms for copper cations on ilerite samples are shown in Fig. 5. The thermal effects obtained when copper nitrate interacted with ilerite samples were determined in separate calorimetric experiments. The net quantitative effects (Q_{res}) for each ilerite–copper interactions (Q_{tit}) were obtained after subtracting the cation dilution effect (Q_{dil}), as given by Eq. (2).

$$\Sigma Q_{res} \Sigma Q_{tit} - \Sigma Q_{dil} \quad (2)$$

These thermal effects from the complete thermodynamic cycle for this series of interactions involve a suspension (sp) of ilerite (il) in aqueous (aq) solution with divalent copper (Cu^{2+}) and are represented by the following thermodynamic cycle:

$$il_{(sp)} + Cu^{2+}_{(aq)} = Cu - il_{(sp)}; Q_{tit} \quad (3)$$

$$il_{(sp)} + nH_2O = il.nH_2O_{(sp)}; Q_{hyd} \quad (4)$$

$$Cu^{2+}_{(aq)} + {}_nH_2O = Cu^{2+}.nH_2O_{(aq)}; Q_{dil} \quad (5)$$

$$il.nH_2O_{(sp)} + Cu^{2+}.nH_2O_{(aq)} = Cu - il_{(sp)} + 2nH_2O); Q_{res} \quad (6)$$

An advantage of the calorimetric titration for such systems in heterogeneous conditions is the simultaneous determination of equilibrium and enthalpy data, after adjusting the net thermal effects to a mathematical model. Through these values, the Gibbs energy and the entropy for this system can also be calculated. For the present case, the net thermal effect obtained from the calorimetric titration is given by Eq. (2) based on Eq. (6). Using the appropriate formalism [18,30,31], the enthalpy involved in the formation of a monolayer can be obtained for each process, which enables the calculation of the molar enthalpy. From K values the Gibbs energy was obtained for interactions and the entropy was calculated from the enthalpy and Gibbs energy. These values are listed in Table 2.

The enthalpic data are endothermic for both studied interactions and the value presented for the aluminum containing sample is higher than that of pure silica ilerite, 2.92 ± 0.01 and 1.5 ± 0.02 kJ mol^{-1}, respectively. To explain the high enthalpic value for the Na–[Al]il sample some considerations are presented about the process: (i) the exothermic copper sorption with possible species Si–OH, Si–O^- and Al–O^-; (ii) the endothermic interaction of sodium cations and sites of ilerite layer; (iii) accessibility of sites

Table 1
Number of moles sorbed (N_f) from the Langmuir (n_s an K_L), the Freundlich (n_F and K_F) and the Temkin (n_T and K_T) isotherms with parameters and determination coefficients (R^2) for the interaction of copper with layered ilerites, Na-il and Na–[Al]il samples (Sple) at 298 ± 1 K.

Sple	N_f	Langmuir			Freundlich			Temkin		
		n_s	K_L	R^2	n_F	K_F	R^2	n_T	K_T	R^2
Na-il	10.1	9.9	126	0.91	12.7	8.4	0.96	0.87	157430	0.98
Na–[Al]il	8.4	7.9	10.1	0.94	11.8	6.2	0.96	0.83	10112	0.96

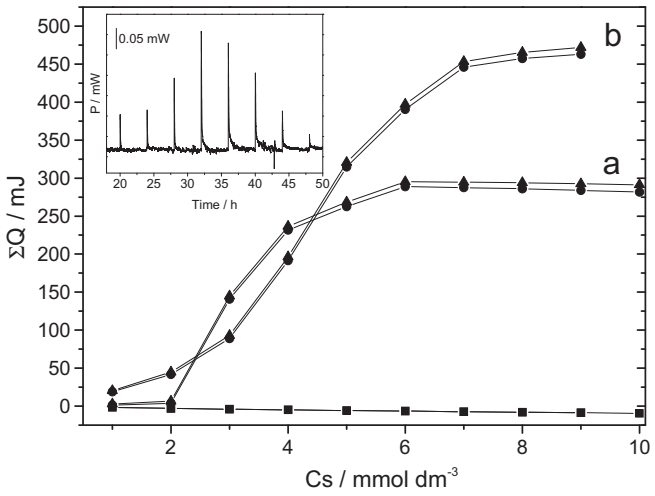

Fig. 5. Resulting (●) and total (▲) thermal effects of the copper sorption on layered Na-il-216 (a) and Na–[Al]il-216 (b)samples and the dilution effect (■) at 298.15 ± 0.20 K. Inset, the power vs time plot for Na–[Al]il-216.

Table 2
Enthalpy, Gibbs energy and entropy for the interaction of copper sorbed on Na-il and Na–[Al]il samples (Sple) at 298.15 ± 0.20 K.

Sple	ΔH (kJ mol^{-1})	ΔG (kJ mol^{-1})	ΔS (J K^{-1} mol^{-1})
Na-il	1.54 ± 0.02	−4.2 ± 0.4	19 ± 1
Na–[Al]il	2.92 ± 0.01	−4.7 ± 0.5	25 ± 1

and (iv) the side reactions of copper species. Two properties contribute for the difference in enthalpic value that is the Lewis and the Brönsted site strengths, caused by aluminum insertion into the silicic network. This process generates one extra negative charge and changes the interactive energy between the available sites and the species with copper cations. For most positive species the interactions with aluminosilicates are stronger than for silicates, especially due to the presence of sodium [32]. Morphology and accessibility also take an important role in calorimetric results, such as easier access that improves the sorption process, allowing maximum capacity. As a result of its thinner crystallites, Na-il has the first titration thermal effect as the most intense enthalpic event and reaches saturation before Na–[Al]il, which is thicker than the analogous silicate. The power against time plot for copper sorption in Na–[Al]il is shown at an inset in Fig. 5, where a very interesting profile is presented. The increase of thermal effect is followed by a decrease after four additions, as indicated by the previous interactions, as it is supposed to occur on the external surface. As the titration progresses with copper concentration increasing, the swelling process starts and sodium release becomes easier. After some exfoliation process due to copper exchange, most sorption sites are occupied, thus the energy for each addition decreases.

The negative Gibbs energy values indicate that a spontaneous process of copper ionic exchange with ilerite samples has occurred, as previously observed for other interactive processes [33,34].

Both systems presented positive entropic values, as shown in Table 2, which are also consistent with previously reported results [33,34]. These values suggest disorganization increases, due to either the exfoliation process or the increase of free species, mainly for two sodium cations that are released for each copper cation. Thus, Na-il and Na–[Al]il present entropic values of 19 ± 1 and 25 ± 1 J mol^{-1} K^{-1} for copper cation interactions. The higher value for the aluminum containing sample should be due to the total exchangeable cations being 9.4 instead of 8.0, and to the interaction strengths near aluminum sites, that reflect on layer exfoliation extension, with a very higher degree for Na–[Al]il as confirmed by XRD.

In summary, the isotherm curves and thermodynamic data indicate ionic exchange and precipitation, which process is entropically dominated and is more accentuated for Na–[Al]il, due to the presence of stronger acidic sites. This set of thermodynamic data associated with low endothermic values for spontaneous reactions, as expressed by negative Gibbs energy and favorable from the entropic point of view, reflect weaker interactive processes, as represented by ionic exchange, as observed for other systems [35,36].

3.3. Structural changes on sorption

The thermodynamic data for this system suggested that the favorable entropic values govern this process, and this fact can be associated with some expected structural changes. In order to demonstrate these changes, the XRD measurements of copper samples were performed and are shown in Fig. 6. For comparison purposes sodium silicate (a), aluminosilicate (c) and copper ilerite (c and d) samples are presented. Ilerite peak intensity referring to the basal distance of 1.1 nm is related to the lamellar staking order degree. After copper sorption strong exfoliation is noticed (b and d) with almost complete disorganization for the aluminosilicate sample (d).

For the Cu-il XRD diffractogram (b) a decrease in intensity is drastically observed for peaks at 7.98, 15.7, 15.9, 18.5, 21.7, 24.1–29.2, 32.3 and 38.2 2θ degrees, referring to the planes 001, 101, 002, 10−2, 102, 130, 20−1, 10−3, 210, 032, 20−2, 023, 103, 041, 004 and 14−3, respectively. Furthermore, the peak at 17.4 2θ degrees referring to plane 012 disappeared. All these changes indicate a strong exfoliation process due to sodium exchange by copper. Chemical analysis reveals the anhydrous average formulas of $(CuO)_4Cu_2Na_3Si_{32}O_{64}(OH)_8$ and $CuOCu_{3.8}Na_{1.2}Al_{0.8}Si_{31.2}O_{64}(OH)_{8.8}$ for Cu-il and Cu–[Al]il, respectively. The amount of copper incorporated is in agreement with that observed by sorption experiments. The amount of copper exchangeable or precipitated is indicated as Cu_n and CuO, however the extension of oxide groups are more complex and are discussed further.

The structural changes for Cu–[Al]il were more pronounced than for the precursor analogous silicate. The XRD pattern (d) shows that the intensity decreases for all peaks and also show

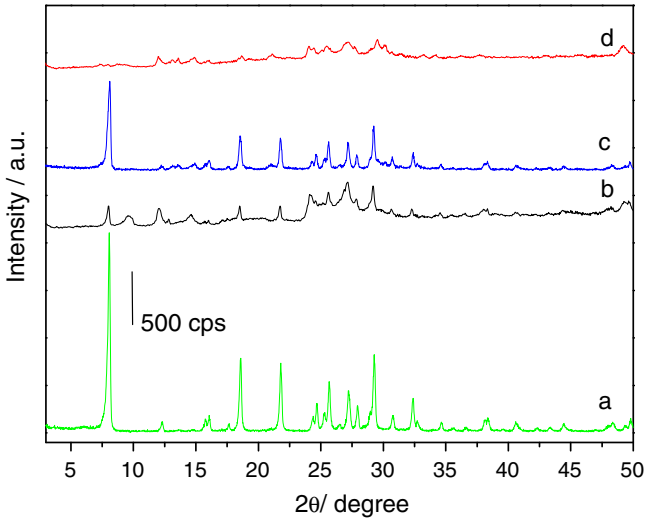

Fig. 6. XRD-patterns of Na-il (a), Cu-il (b), Na–[Al]il (c) and Cu–[Al]il (d)samples.

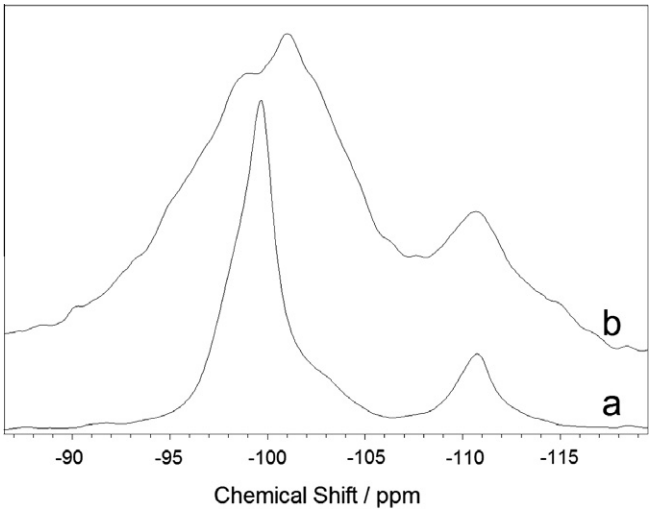

Fig. 7. ^{29}Si NMR spectra of Cu-il (a)and Cu–[Al]il (b) samples.

the disappearance of some, especially the one located at 8.10 2θ degrees, that corresponds to the 001 plane reflection, and to the basal distance. Thus, these changes indicate an almost complete exfoliation process, with no thick crystals of ilerite silicate remaining. These data are in very close agreement with entropy results, as observed for Cu–[Al]il that presents a higher disorder degree than Cu-il. The absence of extra peaks confirms that no new phases were formed with crystals large enough to be observed by XRD.

The layer structure integrity after copper sorption was investigated by ^{29}Si NMR for Cu-il and Cu–[Al]il spectra as shown in Fig. 7. For both materials no chemical shifts displacements were observed, which indicate the structural silicon positions remain after copper sorption, with chemical shifts at −99 and −110 ppm, attributed to Q^3 and Q^4 sites, respectively. For the incorporated aluminum sample (curve b), very strong broadenings for all chemical shifts were observed with Q^2 at −94 ppm and Q^3 at 98 and 101 ppm overlapped signals. This spectral change is due to the local disorder of neighbor atoms other than silicon, copper in this case. Consequently the Q^4 site was not affect in the same way, due to the smaller influence of the surrounding environment. These results also reinforce the higher exfoliation degree of Cu–[Al]il sample over Cu-il.

Transmission and scanning electron microscopy images of ilerite samples are shown in Fig. 8. The silicate material before copper sorption is shown in Fig. 8a, presenting the typical layered morphology for such structure, in good agreement with other SEM results [24], giving rectangular particles with dimensions from 2 to 6 μm each side and widths from tens to hundreds of nm, which means groups of a few tens of lamella. However, many smaller particles were observed, probably broken parts of the crystals that present all dimensions less than 100 nm. Atomic observation was not achieved, due to ilerite quick amorphization with the focused electron beam. After copper sorption the morphology changes in some aspects, while higher dimensions, *a* and *b* axis, remain almost the same. Exfoliation effects were noticed as predicted by XRD and calorimetric results. Also SEM images, inserted in Fig. 8b and c, indicate a decrease in particle organization, which means some exfoliation for layered materials. Thinner crystallites, about 10 to 60 nm, were observed as shown in Fig. 8b. Based on this particle it is possible to visualize three groups of four lamella separated by spaces of 1.4 nm. Also many circular and ellipsoidal particles are observed with average diameters of 2.9 nm for the ilerite particle. These clusters are probably copper oxide and hydroxide, located at interlayer spaces and on the external surface. Nanoparticles are distributed homogeneously on ilerite for the Cu–[Al]il sample, as shown in Fig. 8c. A similar profile of the analogous silicic compound is absent, but with more lamellar disorganization and higher copper precipitation, small particulates and diameters near to 10 nm begins to appear. The formation of higher clusters is an important issue in the exfoliation process that occurs strongly on the aluminosilicate material, which was observed by different characterization techniques such as XRD, TEM and isothermal calorimetric titration.

3.4. X-ray absorption spectroscopy analyses

Copper sorbed on Cu-il and Cu–[Al]il samples was investigated by XAS for solids saturated with solutions of this cation, in similar condition as was observed for the saturation regions of the Langmuir isotherms.

The normalized Cu K-edge XANES spectra obtained for both samples are shown in Fig. 9A, with very similar shapes. Comparing the peaks at the post-edge position, the spectrum of Cu–[Al]il sample (9b) has slightly less defined oscillations around α and β regions, though the spectra for the samples look like each other. In the pre-edge region, inserted on the right hand side in Fig. 9A, the spectra presented some differences, such as a less defined 1s → 3d peak transition for the Cu–[Al]il sample than that observed for Cu-il sample. The partially 1s → 3d dipole-forbidden electronic transition produced a weak peak at ~8973 eV. Based on this energy, the peak is a fingerprinting of copper species in the oxidation state of 2+ [15,37]. The tetragonal distortion of

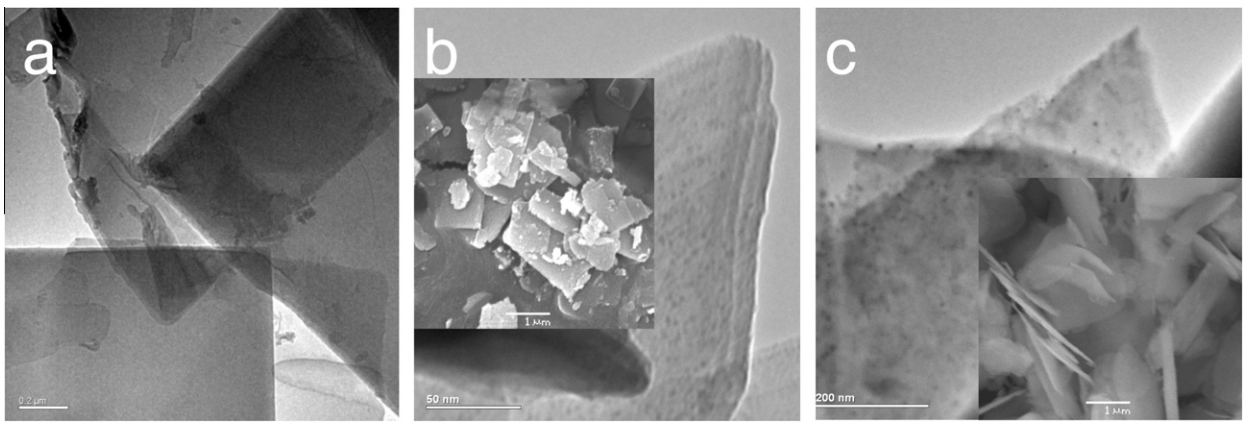

Fig. 8. TEM images of Na-il (a), Cu-il (b) and Cu–[Al]il (c), the insert images are SEM.

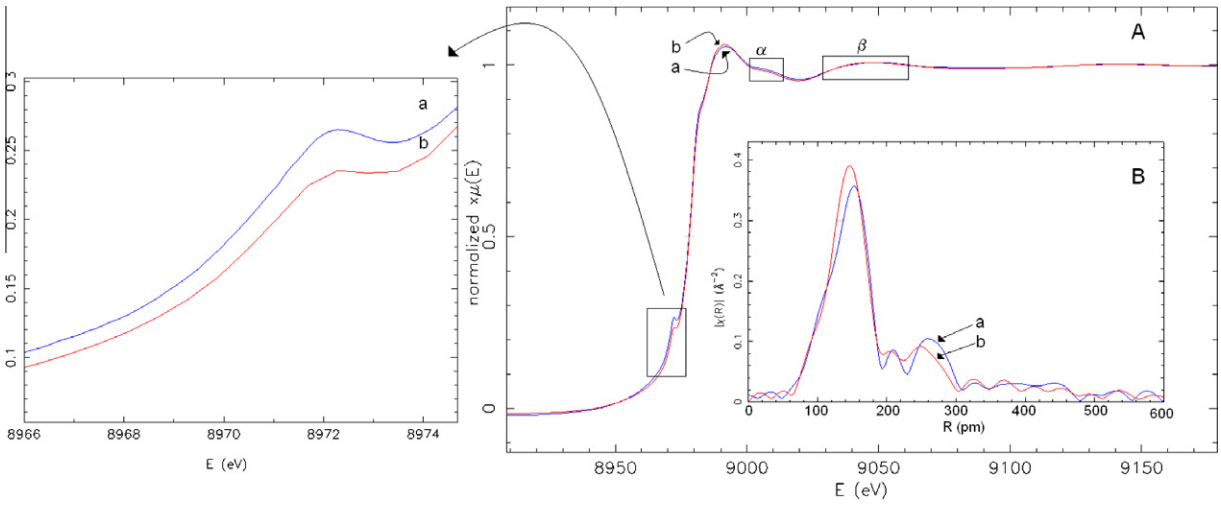

Fig. 9. (A) CuK-edge XANES spectra obtained for Cu-il (a) and Cu–[Al]il (b) and (B) magnitudes of the Fourier transforms of EXAFS spectra.

hexacoordinate copper species can be well identified by the investigation of the XANES spectrum at the CuK-edge due to the 1s electronic transitions of the metal locating in this region [38]. Thus, analyzing 1s → 3d peak resolutions in Fig. 9A, it is possible to conclude that the CuO_6 unit in Cu-il sample had lower distortion from tetragonal symmetry compared to the copper sites in the Cu–[Al]il sample [38].

The two main peaks positioned at 8981–8991 eV in the pre-edge are ascribed to the dipole-allowed 1s → 4p and 1s → *continuum* electronic transitions, respectively. The split in these peaks is only expected when copper is coordinated in a distorted octahedron [39]. The Jahn–Teller distortion predicts that this split takes into account the d^9 electronic configuration of divalent copper [40]. For this metal electronic configuration in an octahedral field, the three electrons are located in the e_g level with d_{z^2} and $d_{x^2-y^2}$ orbitals, whose double degeneracy is removed in order to stabilize one of these orbitals, which is done by lengthening either the two axial or the four equatorial bonds. The distorted octahedron with a shorter equatorial O–Cu–O distance feels a higher electric repulsion along *x* and *y* axes due to the ligand-field stabilization energy. So, as a consequence, the 1s → $4p_{x,y}$ transition takes place at a higher energy value than the energy shift of the 1s → $4p_z$ transition [41]. For the layered materials that were employed as sorbents of metal ions, this information is fundamental to investigate any relation between final coordination of the ligands and the thermodynamic parameters for sorption, associating final electronic configuration with the reversibility of the reaction.

From the XANES spectra and their derivative analyses, the divalent copper in Cu-il and Cu–[Al]il samples resembles that observed in the $Cu(OH)_2$ compound, as a hydroxyl-bridged form. In fact, copper nitrate in aqueous solution readily dissociates to give NO^{3-} and Cu^{2+}, in which the hydroxylation reaction yields $Cu(OH)_2$ [42]. The EXAFS spectra analyses for Cu-il and Cu–[Al]il samples and their simulations, considering theoretical standard phase and amplitude functions, were done in order to obtain a better refinement in the investigation of the copper species present in those layered materials.

Considering as first and second spheres the Cu–O and Cu–Cu bonds, respectively, as shown in Fig. 9B, present the magnitudes of the Fourier transforms of EXAFS spectra for Cu–[Al]il and Cu-il layered materials. The distances and the coordination numbers for both spheres are listed in Table 3, with that for the first region of the R in Fig. 9B corresponding to the backscattering due to oxygen atoms (80–260 pm). The main peak is attributed to the equatorial copper-oxygen bonds ($Cu–O_{eq}$) and the secondary peak contains information concerning the axial bonds ($Cu–O_{ax}$). In the R region for Cu–[Al]il, the amplitude and the position of the two peaks are distinct from those observed for the Cu-il sample. As predicted by Jahn–Teller distortion and verified by the presence of 1s → 4p transitions in the XANES spectra, the axial and equatorial distances could be calculated. The EXAFS simulations corroborated with the *R* analyses for both ilerite samples. For both, exactly the same equatorial distances were calculated, 196 pm, with 3.9 and 4.0 as coordination numbers for Cu-il and Cu–[Al]il samples, respectively. However, the best fit for the aluminum containing sample also presented a second different Cu–O equatorial distance of 189 pm. This smaller distance for the aluminosilicate sample suggests a stronger interaction between copper and oxygen atoms bonded to aluminum atoms. The axial distances of 234 and 247 pm were found for Cu-il and Cu–[Al]il, respectively, with 1.8 coordinating atoms for both materials.

Table 3
Copper-oxygen and copper–copper distances when the cation is sorbed on layered Na-il and Na–[Al]il samples (Sple), for atoms in equatorial (eq) and axial (ax) positions, with number of coordinations in parenthesis, calculated from EXAFS data.

Sple	$Cu–O_{eq}$ (pm)	$Cu–O_{ax}$ (pm)	$Cu–Cu_{eq}$ (pm)	$Cu–Cu_{ax}$ (pm)
Na-il	196 (3.9)	234 (1.8)	291 (2.3)	413 (4.3)
Na–[Al]-il	189 and 196 (4.0)	247 (1.8)	329 (2.4)	489 (4.5)

The second region of the *R* for both samples shown in Fig. 9B corresponds to backscattering due to copper atoms with 260 to 390 pm. The presence of Cu–Cu interactions in the *R* of the layered materials means that copper is coordinated either as a precipitated cluster or as a multinuclear complexation on the surface, whose coordination number correlates to the number of metal atoms in the cluster surrounded by oxygen atoms. The first situation for the Cu–[Al]il sample, in which the best curve-fitting analysis was done with two distances Cu–Cu, 329 and 469 pm, with 2.4 and 4.5 coordination numbers, respectively. These coordination numbers suggest a similar distorted octahedron with second Cu–Cu distance higher than the CuO_6 planar double bridged octahedron. The growth of the original cell from the Cu–[Al]il sample did not exactly approach that of a $Cu(OH)_2$ fitting model. This differential must be related to specific constrains imposed for the growth of CuO_6 units by the surface of this modified layered material. EXAFS

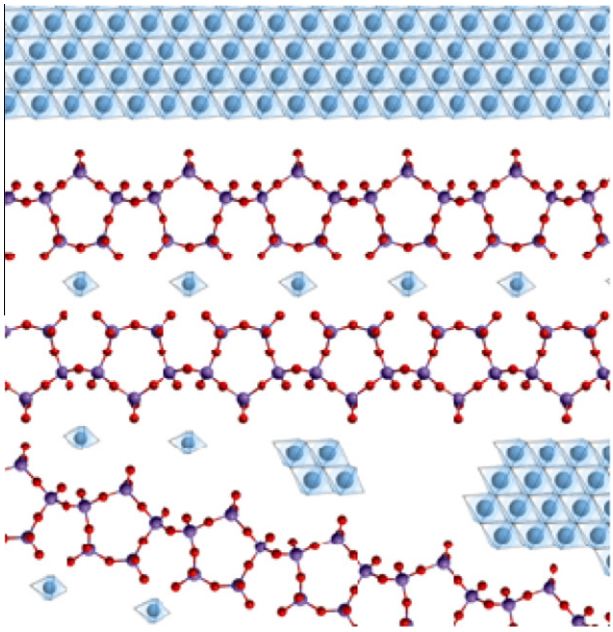

Fig. 10. Schematic model for Cu-ilerite samples, with representation of oxygen (●), silicon or aluminum (●) atoms and hydrated or copper oxides (●).

simulations for the Cu-il sample had a Cu–Cu peak with two distances at 291 and 413 pm, with coordination numbers of 2.3 and 4.3, respectively, having much more similarities to $Cu(OH)_2$-like multinuclear complexes [43].

Considering the high surface coverage of the cations sorbed on both modified layered materials, the presence of isolated and cluster complexes was expected. Sorbed cations on oxide surfaces at high surface concentration [43–45] undergoes changes from mononuclear to multinuclear sorptions and finally to surface precipitation. The sorbing of metal ions took place through hydroxo-bridges at high surface coverage [42,46,47]. In view of this fact, copper sorptions on Cu–[Al]il and Cu-il are present as precipitated clusters and hydrated cations on the surface and agreement with XAFS, TEM and calorimetric results is achieved. Also samples after copper sorption presented potential application in catalysis [10–12].

Based on all observed results, a structure model is proposed in Fig. 10, that consists of some ilerite layers, well organized and parallel to each other, while some lamella are disordered in relation to the next one. Copper species are found as isolated exchangeable cations and as precipitated clusters, as illustrated.

4. Conclusions

The synthesized precursor layered silicate ilerite in sodium form had the element aluminum successfully incorporated in the silicic network, to give a final compound with high crystallinity. Different crystallization pathways were detected for the synthesis with or without aluminum, going from amorphous to ilerite phase or transformed to another phase, which is very similar to magadiite. These differences reflect on morphology and, consequently, on copper sorption capacity. The isomorphic substitution of silicon by aluminum atoms, as also observed in zeolitic systems, generates Brönsted sites on the surface, whose acidity strength and the morphology are demonstrated by differences in copper sorption. The results indicate that copper species interact with the layered lamellar silicates and, for the sample with stronger acidity, bond distances become smaller. XAFS and calorimetric results are in agreement with acid–base principles, as they were described for these systems. The stronger interaction of Na–[Al]il with copper cations through ionic exchange and the subsequent precipitation of copper caused exfoliation at a higher degree than that observed on Cu-il, in agreement with the entropic results. Distances for first and second coordination spheres were calculated for both materials and agree with theoretical results.

Acknowledgements

The authors are indebted to CAPES, CNPq and FAPESP for fellowships and financial support, and also LME-LNLS and MAX-Lab for TEM and XAS measurements and technical support. Also Dr. Alviclér Magalhães is acknowledged for NMR measurements.

References

[1] Z. Wang, T.J. Pinnavaia, J. Mater. Chem. 13 (2003) 2127–2131.
[2] M. Borowski, O. Kovalev, H. Gies, Microporous Mesoporous Mater. 107 (2008) 71–80.
[3] G. Pál-Borbély, A. Auroux, Stud. Surf. Sci. Catal. 94 (1995) 55–62.
[4] G. Borbély, H.K. Beyer, H.G. Karge, W. Schwieger, A. Brandt, K.-H. Bergk, Clays Clay Miner. 39 (1991) 490–497.
[5] U. Brenn, H. Ernst, D. Freude, R. Herrann, R. Jähnig, H.G. Karge, J. Kärger, T. König, B. Mädler, U.-T. Pingel, D. Prochnow, W. Schieger, Microporous Mesoporous Mater. 40 (2000) 43–52.
[6] S. Vortmann, J. Rius, S. Siegmann, H. Gies, J. Phys. Chem. B 101 (1997) 1292–1297.
[7] A. Corma, Chem. Rev. 97 (1997) 2373–2419.
[8] S. Wojciech, F. Roessner, Clays Clay Miner. 59 (2011) 95–105.
[9] M. Valko, H. Morris, M.T.D. Cronin, Curr. Med. Chem. 12 (2005) 1161–1208.
[10] J. Valyon, W.K. Hall, J. Phys. Chem. 97 (1993) 1204–1212.
[11] E.M. Alayon, M. Nachtegaal, M. Ranocchiari, J.A. van Bokhoven, Chem. Commun. 48 (2012) 404–406.
[12] G. Giordano, S. Perathoner, G. Centi, Catal. Today 124 (2007) 240–246.
[13] G.C. Petrucelli, M.A. Meirinho, T.R. Macedo, C. Airoldi, Thermochim. Acta 450 (2006) 16–21.
[14] S.A.M. Critter, J.D. Simoni, C. Airoldi, Thermochim. Acta 232 (1994) 145–154.
[15] H. Dathe, A. Jentys, J.A. Lercher, Phys. Chem. Chem. Phys. 7 (2005) 1283–1288.
[16] H.R. Oswald, A. Reller, H.W. Schmalle, E. Dubler, Acta Cryst. C 46 (1990) 2279–2287.
[17] T.R. Macedo, C. Airoldi, New J. Chem. 33 (2009) 2081–2089.
[18] K.S. Sousa, E.C. Silva Filho, C. Airoldi, Carbohydr. Res. 344 (2009) 1716–1723.
[19] G.N. George, I.J. Pickering, EXAFSPAK-A Suite of Computer Programs for Analysis of X-ray Absorption Spectra;, SSRL, Stanford, CA, 1993.
[20] F. Jalilehvand, D. Spångberg, P. Lindqvist-Reis, K. Hermansson, I. Persson, M. Sandström, J. Am. Chem. Soc. 123 (2001) 431–441.
[21] M. Taylor, G.E. Brown Jr., Geochim. Cosmochim. Acta 43 (1979) 61–75.
[22] A.J. Léonard, P. Ratnasamy, F.D. Declerck, J.J. Fripiat, Discuss. Faraday Soc. 52 (1971) 98–108.
[23] P.H. Fuoss, P. Einsenberger, Phys. Rev. Lett. 46 (1981) 1537–1540.
[24] B. Royer, N.F. Cardoso, E.C. Lima, T.R. Macedo, C. Airoldi, J. Hazard. Mater. 181 (2010) 366–374.
[25] I. Wolf, H. Gies, C.A. Fyfe, J. Phys. Chem. B 103 (1999) 5933–5938.
[26] H. Gies, B. Marler, S. Vortmann, U. Oberhagemann, P. Bayat, K. Krink, J. Rius, I. Wolf, C. Fyfe, Microporous Mesoporous Mater. 21 (1998) 183–197.
[27] G.A. Jeffrey, Y. Yeon, Acta Crystallogr. 42 (1986) 410–413.
[28] S. Vortmann, J. Rius, S. Siegmann, H. Gies, J. Phys. Chem. B 101 (1997) 1292–1297.
[29] S.M.C. Menezes, Y.L. Lam, K. Damodaran, M. Pruski, Microporous Mesoporous Mater. 95 (2006) 286–295.
[30] M.G. da Fonseca, J.S. Barone, C. Airoldi, Clays Clay Miner. 48 (2000) 638–647.
[31] C. Airoldi, Y. Gushikem, J.G.P. Espinola, Colloids Surf. 17 (1986) 317–323.
[32] M. Hunger, Catal. Rev. Sci. Eng. 39 (1997) 345–393.
[33] W.H. van Riemsdijk, S.E.A.T.M. van der Zee, Comparison of models for adsorption, solid solution and surface precipitation. Interactions at the soil colloid-soil solution interface, Kluwer, Ritsumeikan, 1991.
[34] O. Yavuz, Y. Altunkaynak, F. Güzel, Water Res. 37 (2003) 948–952.
[35] J.C.P. Melo, E.C. Silva Filho, S.A.A. Santana, C. Airoldi, Thermochim. Acta 524 (2011) 29–34.
[36] C. Airoldi, L.M. Nunes, Langmuir 16 (2000) 1436–1439.
[37] L.S. Kau, D.J. Spira-Solomon, J.E. Penner-Hahn, K.O. Hodgson, E.I. Solomon, J. Am. Chem. Soc. 109 (1997) 6433–6442.
[38] L. Palladino, S. Della Longa, A. Reale, M. Belli, A. Scafati, G. Onori, A. Santucci, J. Chem. Phys. 98 (1993) 2720–2726.
[39] L. Dupont, E. Guillon, J. Bouanda, J. Dumonceau, M. Aplincourt, Environ. Sci. Technol. 36 (2002) 5062–5066.
[40] F.A. Cotton, G. Wilkinson, Advanced Inorganic Chemistry, 5th ed., Wiley Interscience, New York, 1998.
[41] B. Douglas, D. McDaniel, J. Alexander, Concepts and Models of Inorganic Chemistry, 3rd ed., John Willey Inc, New York, 1994.

[42] Y.L. Wei, Y.C. Lee, Y.W. Yang, J.F. Lee, Chemosphere 57 (2004) 1201–1205.
[43] S.F. Cheah, G.E. Brown Jr., G.A. Parks, J. Colloid Interface Sci. 208 (1998) 110–128.
[44] C.J. Chisholm-Brause, P.A. O'Day, G.E. Brow Jr., G.A. Parks, Nature 348 (1990) 528–530.
[45] S.N. Towle, J.R. Bargar, G.E. Brow Jr., G.A. Parks, J. Colloid Interface Sci. 187 (1997) 62–82.
[46] J.D. Morton, J.D. Semrau, K.F. Hayes, Geochim. Cosmochim. Acta 65 (2001) 2709–2722.
[47] Y.L. Wei, Y.W. Yang, N. Cheng, Environ. Sci. Technol. 35 (2001) 416–421.